Measurement of the Superluminal Group Velocity of an Ultrashort Bessel Beam Pulse

I. Alexeev, K. Y. Kim, and H. M. Milchberg

Institute for Physical Science and Technology, University of Maryland, College Park, Maryland 20742

(Received 11 October 2001; published 31 January 2002)

The superluminal group velocity of an ultrashort optical Bessel beam pulse is measured over its entire depth of field, corresponding to $\sim 2 \times 10^4$ optical wavelengths. The method used is to measure the traveling ionization front induced by the pulse.

DOI: 10.1103/PhysRevLett.88.073901 PACS numbers: 42.25.Bs, 42.65.Re, 52.50.Jm

There has been much interest in solutions to the electromagnetic wave equation that are invariant in the plane transverse to propagation. Such solutions, known as Bessel beams, have been called "diffraction-free" [1] although, for beams of finite transverse extent, this property does not apply globally but only locally along an effective depth of field. In that sense, their diffractive spreading is no less than for ordinary Gaussian beams [2]. However, the transverse field profile invariance within the depth of the field allows for useful applications in, for example, imaging [3], nonlinear optics [4], dispersion compensation [5], and the generation of long plasma fibers for the guiding of intense pulses [6–8].

These beams are solutions $E(\mathbf{r}_\perp, z, \omega) = u(\mathbf{r}_\perp, \omega) \times \exp[ik_z(\omega)z]$ to the Helmholtz wave equation $(\nabla_\perp^2 + k_\perp^2)u = 0$, where $k_\perp^2(\mathbf{r}_\perp, \omega) = k^2(\mathbf{r}_\perp, \omega) - k_z^2(\omega)$, $k(\mathbf{r}_\perp, \omega) = n(\mathbf{r}_\perp, \omega)/c$, ω is the light frequency, and $n(\mathbf{r}_\perp, \omega)$ is the refractive index of the ambient medium. Recent experiments have attempted to measure superluminal propagation of microwave Bessel beams over a very small depth of field (20–25 wavelengths), with the resulting artifact that the propagation distance appeared to be nonlinearly increasing with time [9]. In addition, the experimental uncertainties were rather large, and there were several questions about the interpretation of the results [9,10].

In this Letter, we measure the superluminal group velocity of an ultrashort ($\sim$70 fs) optical Bessel beam pulse over its entire depth of field of $\sim 2.3 \times 10^4$ wavelengths, using three diagnostics that monitor the extremely rapid generation of plasma by the propagating beam.

In a uniform medium $n = n(\omega)$, an azimuthally symmetric solution to the Helmholtz equation is the zero order Bessel beam $E(r, z, \omega) = E_0 J_0(k_\perp r) \exp[ik_z(\omega)z]$, where E_0 is the on-axis field amplitude. (The case of transverse index variation has been experimentally and theoretically investigated, where, under certain conditions, resonant behavior is exhibited [8].) Practically, Bessel beams have been produced by phase masks [4,7], a ring-shaped slit followed by a lens [1], or axicons [6,8]. The latter is a conical lens of transparent material or a conical reflecting surface. For the axicon in the form of a conical lens of index n_a in an ambient medium of index n, a plane wave normally entering the flat side will refract at the conical surface, forming a conical wave front which approaches the z axis at an angle $\gamma(\omega) = \sin^{-1}[\sin(\alpha) n_a(\omega)/n(\omega)] - \alpha$, where α is the axicon base angle, giving $k_z(\omega) = k \cos\gamma$ and $k_\perp(\omega) = k \sin\gamma$, where $k = \omega n(\omega)/c$. For a beam of radius R_b incident on the flat side of the axicon, the effective depth of field of the Bessel beam is $z_d \approx R_b(1/\tan\gamma - \tan\alpha)$ [6]. This is the geometric extent of the line focus along the z axis, where the azimuthal contributions of the conical beam mutually interfere.

A pulsed Bessel beam of zero order can be represented by

$$E(r, z, t) = \int_{-\infty}^{\infty} d\omega\, A(\omega - \omega_0) G(z) J_0[k_\perp(\omega) r] \times e^{i[k_z(\omega)z - \omega t]}, \quad (1)$$

where $A(\omega - \omega_0)$ is the spectral amplitude of the incident pulse, ω_0 is the carrier frequency of the pulse, and $G(z) \propto [z I_{\rm in}(\rho(z))]^{1/2}$ is a geometric factor applicable to the range $0 < z < z_d$, which describes the mapping $z(\rho) \approx \rho(1/\tan\gamma - \tan\alpha)$ by the axicon of the input intensity profile $I_{\rm in}(\rho)$ to the focal line [6]. For short pulses, the Bessel beam diameter is limited by the finite pulse width τ rather than the finite input beam aperture, giving in our case approximately $\frac{1}{2} ck\tau/\pi \sim 30$ lobes in the beam profile.

Away from resonances in the axicon glass or in the ambient medium, and for smoothly varying $A(\omega - \omega_0)$, $k_z(\omega)$ can be expanded in a series about $\omega = \omega_0$ to yield, up to the term in the group velocity dispersion (GVD),

$$E(r, z, t) \approx e^{i[k_z(\omega_0)z - \omega_0 t]} \times \int_{-\infty}^{\infty} d\omega\, A(\omega) G(z) J_0(k_\perp r) \times e^{i(1/2)\beta\omega^2 z} e^{i\omega(z/v_g - t)}, \quad (2)$$

where $v_g = (\partial k_z/\partial\omega)^{-1}_{\omega=\omega_0}$ is the group velocity, and $\beta = (\partial^2 k_z/\partial\omega^2)_{\omega=\omega_0}$ is the GVD. Assuming that the dispersion of the ambient gas is negligible, the Bessel beam pulse therefore propagates (in the region $0 < z < z_{\rm d}$) at speed

$$v_g = \frac{c}{n(\omega_0)}\left[\cos\gamma_0 - \frac{\sin\gamma_0 \sin\alpha}{\cos(\gamma_0 + \alpha)} \frac{\omega_0}{n(\omega_0)} \frac{dn_a(\omega_0)}{d\omega}\right]^{-1} = v_p(1 + \delta), \quad (3)$$

where $\gamma_0 = \gamma(\omega_0)$, $v_p = c/[n(\omega_0)\cos\gamma(\omega_0)]$ is the phase velocity, and δ [>0 for normal dispersion $n_a'(\omega_0) > 0$ of the axicon glass] is a small correction showing that the group velocity is greater than the phase velocity. Since $\cos\gamma_0 < 1$, it is immediately seen that the group velocity is greater than the speed of light, $c/n(\omega_0)$, in the ambient medium. Although there has been debate [9–11] about this superluminal effect, it does not constitute a violation of special relativity: Evaluation of the energy flow velocity $v_E = \mathbf{S} \cdot \hat{z}/U$ of the Bessel beam pulse, where $\mathbf{S}$ is the Poynting vector and U is the electromagnetic energy density, gives the *subluminal* result $v_E = [c/n(\omega_0)]\cos\gamma_0$. The Bessel beam is formed from mutual interference of intersecting (and relativity obeying) conical wave fronts. Simple geometric construction shows that the constant phase intersection points (that is, the interference pattern that constitutes the Bessel beam) will move at greater than light speed. We note that the concept of group velocity is still applicable here; it gives the pulse envelope velocity.

Figure 1 is a schematic of the experimental setup. Pulses [100 mJ, $\tau = 70$ fs (FWHM), $\lambda_0 = 800$ nm] from a 10 Hz Ti:sapphire laser system were split by a beam splitter, providing pump (90 mJ) and diagnostic (10 mJ) pulses. The ~3.5 cm diameter pump beam was normally incident on a 2.5 cm diameter BK7 glass axicon with $\alpha = 34.4 \pm 0.3°$ [giving $\gamma(\lambda_0) = 24.2 \pm 0.4°$], and a $2a = 3$ mm diameter hole on its axis. The hole resulted in the Bessel beam focus beginning at $z_{\min} = a(1/\tan\gamma - \tan\alpha) = 2.3$ mm instead of $z = 0$. The ambient gas was argon at 1 atm. Given an input pulse width τ and bandwidth $\Delta\omega$, the axicon-generated Bessel beam pulse width is geometrically stretched to $\tau/\cos\gamma$ (to 70 fs/cos24.2° ~ 77 fs), and compressed by GVD by a maximum amount $\Delta\tau \sim \beta\Delta\omega z_d$ (~−10 fs, for $\beta = -0.020$ fs$^2/\mu$m at $\lambda_0 = 800$ nm [12]). Therefore, for our slightly chirped input pulses, the effects of geometric stretching and GVD roughly cancel, leaving the pulse width effectively unchanged.

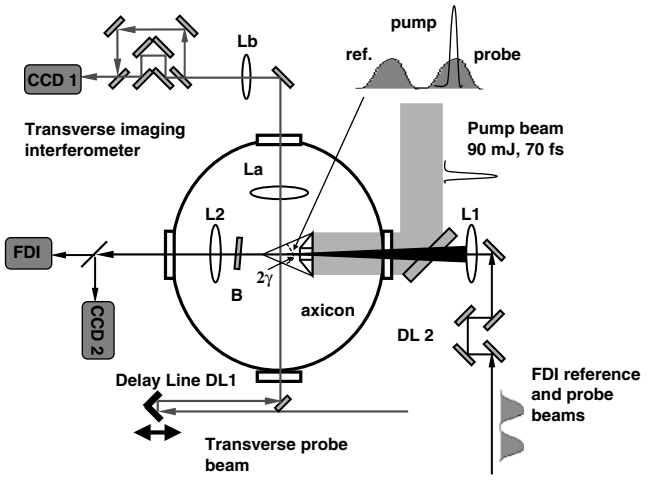

FIG. 1. Experimental setup, showing pump and probe beam paths, and the diagnostics used to measure the ionization front. DL1—delay line for transverse imaging interferometer; DL2—delay line for longitudinal reference and probe pulses at 400 nm; B—beam blocker for 800 nm pump beam; L1—lens for focusing of twin UV pulses; L2—lens for imaging of UV pulses; L_a and L_b—two-lens imaging system for transverse interferometer; FDI—frequency domain interferometer.

The 10 mJ diagnostic pulse was split further by a pellicle, with 1 mJ directed transversely through the axicon focal region, through a two-lens imaging system (L_a and L_b), and into a modified Mach-Zehnder interferometer. The two-lens system imaged the plane containing the Bessel beam focus (and the resulting plasma) onto the charge coupled device camera CCD1 at the interferometer output. By varying the probe pulse delay (DL1) with respect to the pump pulse, a sequence of interferograms of the plasma evolution was obtained, with time resolution limited by the probe pulse width of $\tau_{\text{probe}} = 70$ fs (for the case where the plasma diameter is smaller than $c\tau_{\text{probe}}$). Electron density profiles were obtained from phase extraction [7,13] of these interferograms. By blocking one arm of the interferometer, phase contrast images (shadowgrams) of the interaction region could be obtained.

The remaining ~9 mJ was directed to a thin KDP (potassium dihydrogen phosphate) crystal, producing a frequency doubled ultraviolet (UV) pulse with center wavelength 400 nm and bandwidth ~4 nm. The UV beam was sent to a Michelson interferometer (not shown) to create equal energy reference and probe pulses with a fixed time separation, after which they were chirped to ~1 ps by a 25 mm thick piece of dispersive SF4 glass, producing a linear mapping between the frequency and the time domains, and allowing single-shot measurements of plasma evolution. The pulses were then sent through delay line DL2, and weakly focused with lens L1 ($f = 50$ cm) through the 3 mm hole in the axicon, overfilling the axicon line focus. The twin UV pulse timing was arranged so that the first (reference) UV pulse arrived in the interaction region before the pump pulse, which arrived during the second (probe) UV pulse. After removal of the pump light by beam splitter B, lens L2 ($f = 15$ cm) formed UV images of the plane $z = z_d \approx 1.9$ cm on camera CCD2 and on the entrance slit of a frequency domain interferometer (FDI) [14], here a 1 m imaging spectrometer. The image collected by the FDI is resolved on orthogonal frequency (time) and 1D space axes, yielding a time and 1D space-resolved record of the plasma-induced phase shift. Images (CCD2) of the probe pulse at the exit plane of the interaction region were obtained by blocking the UV reference pulse and removing the SF4 chirping glass.

The generation of plasma by the Bessel beam pulse occurs through field ionization of the ambient gas. The peak intensity of the beam in its central lobe is $\sim 3 \times 10^{14}$ W/cm^2 (from high magnification images of the focal intensity profile [7]), which is sufficient to generate Ar^{1+} from neutral Ar [15]. The field ionization rate per atom is given by [16] $(\tau_{Z-1\to Z})^{-1}$ s^{-1} $= 8 \times 10^{16}(2l + 1)E_H^{1/2}\chi_H^{1/4}[2\chi_H^{3/2}E_H^{-1}]^{2n_{\text{eff}}-1}e^{-(2/3)\chi_H^{3/2}E_H^{-1}}$, where Z is the resulting ion charge, E_H is the laser field normalized to the atomic field seen by the ground state electron in hydrogen, χ_H is the ionization potential normalized to that of hydrogen, $n_{\text{eff}} = Z\chi_H^{-1/2}$ is the effective principal quantum number, and l is the orbital quantum number for electrons in the outer shell. For ionization of neutral argon at $I_{\text{peak}} = 3 \times 10^{14}$ W/cm^2, $l = 1$, $\chi_H = 1.16$, and $E_H \sim 0.1$, giving $\tau_{0\to 1} \sim 4$ fs, well within the pulse envelope. Additional ionization is negligible ($\tau_{1\to 2} \sim 1.8$ ps). The result is the localization of ionization to the reference frame of the moving pulse; the ionization front moves at the pulse group velocity. The generated free electrons and singly charged ions form a thin, extended plasma track behind the pulse, which persists even after the pulse has left the focal region. This is analogous to a cloud chamber track left by an energetic particle.

Figure 2 shows a series of side-view shadowgrams of the plasma generated by the propagating Bessel beam pulse, taken at increasing relative delay of the transverse probe pulse. The plasma track is easily identifiable, with the ionization front propagating away from the axicon vertex. Inset 2(a) shows an axial lineout of one of the gray scale images, with a rising edge of ~ 25 μm, consistent with the 70 fs probe resolution. The same edge behavior is replicated at all delays, allowing an accurate measure of the group velocity $\Delta L/\Delta t$, where ΔL is the distance propagated by the midpoint of the rising front, and Δt is the delay. The measured ionization front speed was $v_{\text{front}} = (3.332 \pm 0.036) \times 10^{10}$ cm/s $= (1.111 \pm 0.012)c$. The error represents the maximum deviation from the least squares fit to the data, and originates from random uncertainties in readings of the DL1 micrometer, and a systematic uncertainty in the image spatial calibration. This result is in excellent agreement with the theoretical value (including the ambient gas) of $v_g = (1.105 \pm 0.003)c$, where the theory uncertainty is from the measurement of α. Comparison of v_{front} to the theoretical value $v_p = (1.096 \pm 0.003)c$ gives an indication that the contribution δ in Eq. (3) is not ignorable. Inset 2(b) shows radial electron density profiles from transverse interferometry, taken near the beginning of the interaction region at ~ 0 ps (immediately after the passage of the pulse), and 200 ps later (a time $t > z_d/v_g$, after the pulse has left the focus). The plasma column left by the pulse is almost stationary, consistent with the minimal thermal heating provided by the femtosecond pump pulse [6]. The peak average ionization is $Z \sim 1$, obtained by dividing the peak electron density by the gas number density at 1 atm, and agreeing with the field ionization prediction. Recombination decay of the electron density begins at ~ 1 ns, well after the pulse.

The UV beam diagnostics relied on the superluminal pump pulse (moving at v_g) outrunning a copropagating UV probe pulse [moving at $v_{\text{probe}} \approx c/n(2\omega_0)$] and blowing a hole in it. In one limit, if the probe pulse is injected

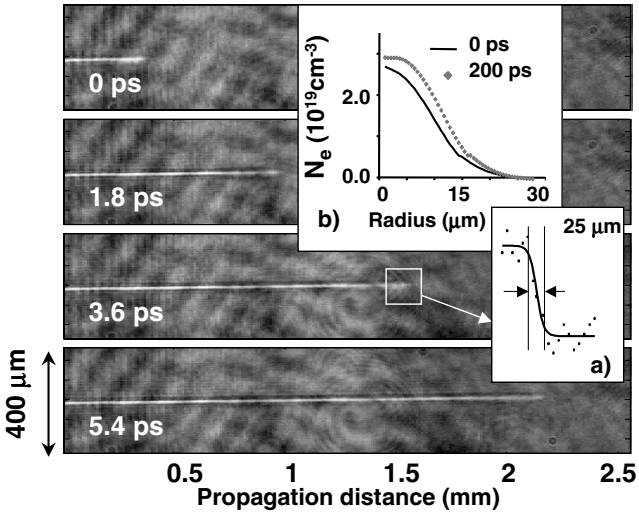

FIG. 2. Side-view shadowgrams of Bessel pulse-induced ionization track taken at four successive delays (40 delays were used to determine the propagation speed). The delay time scale has been shifted so that zero delay corresponds to the top image. Inset (a) shows an axial lineout of the ionization front, and inset (b) shows electron density profiles extracted from interferograms at times coincident with the pump pulse (~ 0 ps), and long after it has left the focal region (200 ps).

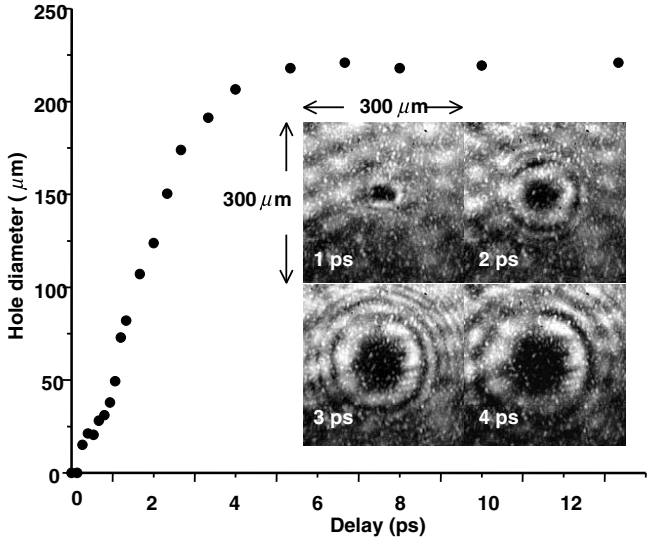

FIG. 3. Diameter of refraction-induced "hole" in probe UV pulse induced by superluminal ionization front, versus pump-probe delay. The delay time scale has been shifted so that zero delay corresponds to undetectable refraction. Inset: Images of probe pulse at end of axicon focus at selected delays.

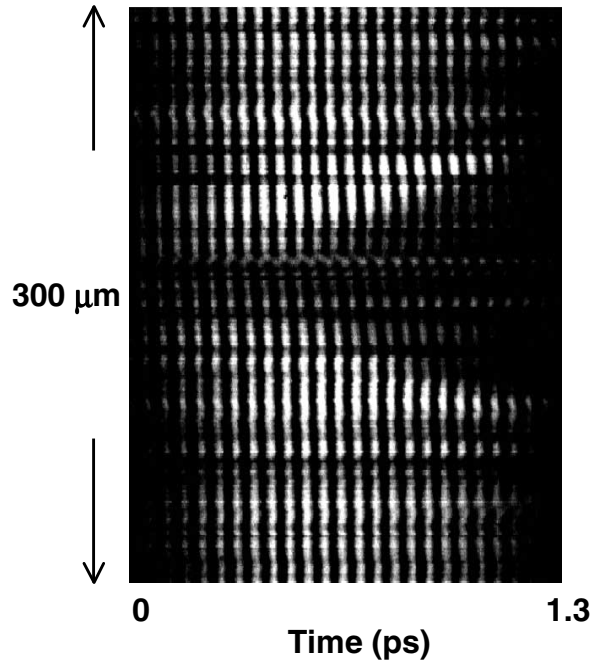

FIG. 4. Single-shot FDI image, showing time resolved refraction of the probe pulse in a ~1 ps window. The time window is too short to show the saturation of refraction. The opening of the conelike structure toward increasing times is a direct demonstration of the superluminality of the Bessel beam pulse.

into the interaction region coincident with or behind the Bessel beam pump pulse, it will propagate over the *full* length $L = z_d - z_{\min}$ of the generated plasma column, and a CCD2 image of the probe beam at plane $z = z_d$ would show a "hole" where the plasma column is located. The hole results from refraction of probe pulse energy away from the plasma axis, and it increases in diameter with the length of plasma Δz_{plasma} encountered. In the opposite limit, the probe pulse is injected with enough of a head start that the superluminal pump can never catch up. Then $\Delta z_{\text{plasma}} = 0$, and no hole is induced in the probe. Figure 3 shows a plot of hole diameter versus pump-probe delay. Images from four delays are shown in the inset. At delay $\Delta t = 0$ there is no hole, and by $\Delta t > \Delta t_{\text{sat}} \sim (5 \pm 1)$ ps the hole diameter saturates, as expected from the almost stationary plasma which trails the pump pulse [see inset 2(b)]. In the intermediate delays, where $\Delta z_{\text{plasma}} < L$, the pump catches up to and passes the probe. For our purposes, the detailed variation of the hole diameter with delay is less important than the value of Δt_{sat}, which is related to the pump pulse group velocity (or the ionization front speed) by $\Delta t_{\text{sat}} = L(v_{\text{probe}}^{-1} - v_g^{-1})$. Using $\Delta t_{\text{sat}} \sim 5$ ps, $L = 1.7$ cm, and $v_{\text{probe}} = c$, gives $v_g = (1.10 \pm 0.03)c$, independently confirming the shadowgraphy results of Fig. 2. The error is from uncertainty in identifying a distinct Δt_{sat} to within ± 1 ps.

Finally, we show the result of using the chirped ~1 ps UV pulses with the FDI. At low ambient argon pressure (~50 torr), where the resulting plasma column refracts only weakly, the FDI image allows extraction of the electron density, and this result agrees with that from the transverse interferometer. At 1 atm, refraction removes beam energy from where the fringes would normally be, but one gets a single-shot, time-resolved picture of the refraction. This shows up in the FDI image of Fig. 4 as the cone-shaped shadow, which is a 1D section of a growing hole. While the ~1 ps time window was insufficient to see the hole radius saturate, the gradual opening of the cone to the right of the image (toward higher frequencies and longer times) is a direct demonstration of the superluminal propagation of the pump pulse.

The authors thank J. Fan for useful discussions, and for help with the optical alignment. This work was supported by the Department of Energy and the National Science Foundation.

[1] J. Durnin, J. J. Miceli, and J. H. Eberly, Phys. Rev. Lett. **58**, 1499 (1987).
[2] P. Sprangle and B. Hafizi, Phys. Rev. Lett. **66**, 837 (1991).
[3] J. H. McLeod, J. Opt. Soc. Am. **50**, 166 (1960).
[4] T. Wulle and S. Herminghaus, Phys. Rev. Lett. **70**, 1401 (1993).
[5] H. Sõnajalg and P. Saari, Opt. Lett. **21**, 1162 (1996); H. Sõnajalg, M. Rätsep, and P. Saari, Opt. Lett. **22**, 310 (1997); P. Saari and K. Reivelt, Phys. Rev. Lett. **79**, 4135 (1997); M. A. Porras, Opt. Lett. **26**, 1364 (2001).
[6] C. G. Durfee, J. Lynch, and H. M. Milchberg, Phys. Rev. E **51**, 2368 (1995); S. P. Nikitin *et al.,* Phys. Rev. E **59**, R3839 (1999).
[7] J. Fan *et al.,* Phys. Rev. E **62**, R7603 (2000).
[8] J. Fan, E. Parra, and H. M. Milchberg, Phys. Rev. Lett. **84**, 3085 (2000).
[9] D. Mugnai, A. Ranfagni, and R. Ruggeri, Phys. Rev. Lett. **84**, 4830 (2000).
[10] H. Ringermacher and L. Mead, Phys. Rev. Lett. **87**, 059402 (2001); N. P. Bigelow and C. R. Hagen, *ibid.* **87**, 059401 (2001).
[11] E. Recami, Physica (Amsterdam) **252A**, 586 (1998).
[12] BK7 refractive index data from Schott Optical Glass Catalog, Schott Glass Technologies Inc. (1992).
[13] T. R. Clark and H. M. Milchberg, Phys. Rev. Lett. **78**, 2373 (1997).
[14] E. Tokunaga, A. Terasaki, and T. Kobayashi, Opt. Lett. **17**, 1131 (1992); J. P. Geindre *et al.,* Opt. Lett. **19**, 1997 (1997); C. Siders *et al.,* Phys. Rev. Lett. **76**, 3570 (1996); P. Chessa *et al.,* Phys. Rev. Lett. **82**, 552 (1999).
[15] S. Augst *et al.,* Phys. Rev. Lett. **63**, 2212 (1989).
[16] M. V. Ammosov, N. B. Delone, and V. P. Krainov, Zh. Eksp. Teor. Fiz. **91**, 2008 (1986) [Sov. Phys. JETP **64**, 1191 (1987)].